

NSF CDSE DRAFT 02

Thor, Gibbs, Zeus, the guy who invented sticky notes, Santa Claus*

*North Pole department of ice and snow Fwding address - Department of Chemical and Biochemical Engineering,
Rutgers, The State University of New Jersey, Piscataway, NJ, USA 08854*

Abstract

abstract text goes here ...

Keywords: Population balance model, heteroaggregation, alginate, chitosan, oppositely charged

1. Introduction & Objectives

description of particulate processes and challenges... leads up to our "solution" or start of solution which is what this paper is about

particulate process and how they are half all chem industry

Particulate processes are ones in which a system of discrete species exist, such as a granules or catalysts, that undergo changes in average composition, size, or other pertinent property. Important products that are produced using particulate processes include detergents, aerosols, fertilizers, and pharmaceuticals **need cite? if so cite prakash**. Despite the prevalence of these particulate systems in industry there is a lack of modelling capabilities, to aid in process design, which is due to the complex phenomena of these systems.

**despite being important they are VERY hard to model and study bec of microphenomena.
strain difficulty and added costs to industry bec of this**

The lack of modelling capabilities for these systems has led to industry depending on inefficient production methods which lead to higher costs (Ramachandran et al. (2009)).

**PBM DEM have been helpful for this however but they take long time to solve
in the past when faced with comp heavy tasks scientists have used parallel computing. divide
big prob into small pieces that are simultaneously solved. time to solve is time to solve small piece.**

potential benefits this could have 1. unprecedented accuracy 2. wide adoption of using these models since they are so fast 3. cheaper drugs 4. MPC accurate but in real time 5. parameter estimation for QbD 6. etc.

1.1. Objectives

1. develop 4D PBM that is parallelized spatially and internally for optimal utilization of modern HPC equipment.

2. use ligggths to accurately model micromechanics for processing in Lodgitech granulator.

3. LINK PBM-DEM for best of both worlds and optimal performance. 1-way or if possible 2-way coupling

*Corresponding author

Email address: **santaclaus** (Santa Claus)

27 **2. Background & Motivation**

28 *2.1. Particulate Processes*

29 pharma / particulate processes information prevalence etc
30 difficult physics bec micro phenomena etc
31 as result use time consuming and expensive heuristics or inefficient operation protocol dotdotdot
32 also reason most blah done in batch mode still bec continuous mode compounds complexity of these
33 systems
34 will need to switch to continuous etc
35 segway with need to better understand these systems from a modelling/theory point of view
36 dotdotdot QbD etc

37 *2.2. Modeling*

38 *2.2.1. Discrete Element Modeling (DEM)*

Discrete Element Method is a simulation technique used to monitor the behaviour of each particle as a separate entity compared to other bulk continuum models. This method tracks the movement of each of the particles with in the space, records the collisions of each particle with the geometry as well as with each other and it is also subject to other force fields like gravity (Barrasso and Ramachandran (2015)) This model is based on the Newton's laws of the motion and is expressed as in Equations 1 and 2 :

$$m_i \frac{dv_i}{dt} = F_{i,net} \quad (1)$$

$$F_{i,net} = F_{i,coll} + F_{i,ext} \quad (2)$$

39 In the above equations m_i represents the mass of the particle, v_i represents the velocity of the
40 particle, $F_{i,net}$ represents the net force on the particle, forces on the particle due to collisions and
41 other external forces are represented in $F_{i,coll}$ $F_{i,ext}$ respectively.

42 The distance between each particle calculated at every time step and if the distance between
43 two particles is less than the sum of the radii (for spherical particles) a collision between the two
44 particles is recorded. The tolerance for overlap is low in the normal as well as the tangential direction
45 (Cundall and Strack (1979)). Microscale DEM simulations are computationally demanding and
46 simulations may take upto several days to replicate a few seconds of real time experiments. Many
47 methods have been implemented to increase the speed of these simulations, such as scaling by
48 increasing the size of the particles. These approximations are good in understanding the physics
49 of the system but are not directly applicable to process-level simulations.

50 Thus, this method for granular powder is usually replaced by Population Balance Method
51 (PBM) which is a much quicker approximation as it is a bulk model.

52 *2.2.2. PBM*

53 Population balance models predict how groups of discrete entities will behave on a bulk scale due
54 to certain effects acting on the population with respect to time (Ramkrishna and Singh (2014)). In
55 the context of process engineering and granulation, population balance models are used to describe
56 how the number densities, of different types of particles, in the granulator change as rate processes
57 such as aggregation and breakage reshape particles (Barrasso et al. (2013)). A general form of
58 population balance model is shown here as equation 3.

$$\frac{\partial}{\partial t} F(\mathbf{v}, \mathbf{x}, t) + \frac{\partial}{\partial \mathbf{v}} [F(\mathbf{v}, \mathbf{x}, t) \frac{d\mathbf{v}}{dt}(\mathbf{v}, \mathbf{x}, t)] + \frac{\partial}{\partial \mathbf{x}} [F(\mathbf{v}, \mathbf{x}, t) \frac{d\mathbf{x}}{dt}(\mathbf{v}, \mathbf{x}, t)] \\ = \mathfrak{R}_{formation}(\mathbf{v}, \mathbf{x}, t) + \mathfrak{R}_{depletion}(\mathbf{v}, \mathbf{x}, t) + \dot{F}_{in}(\mathbf{v}, \mathbf{x}, t) - \dot{F}_{out}(\mathbf{v}, \mathbf{x}, t) \quad (3)$$

59 In equation 3 \mathbf{v} is a vector of internal coordinates. For modelling a granulation process \mathbf{v} is
 60 commonly used to describe the solid, liquid, and gas content of each type of particle. The vector
 61 \mathbf{x} represents external coordinates, usually spatial variance. For a granulation process this account
 62 for spatial variance in the particles as they flow along the granulator.

63 talk about kernels - empirical, semi mech, and DEM informed? talking about kernels then
 64 mentioning there is DEM informed could be GREAT SEGWAY to multi-physics models dotdotdot
 65 combined PBM DEM etc.

66 *2.2.3. multi-physics models*

67 general goal of mutli physics is best of two (or more worlds) accuracy of one but the time savings
 68 of another etc.

69 finish with PBM DEM goals and past works? then mention it still can take a long time dotdotdot
 70 SEGWAY into parallel computing?

71 *2.3. Parallel Computing and Computer Architectures*

72 *2.3.1. Overview*

73 The goal of parallel computing is to distribute large amounts of computation across many
 74 compute cores to solve problems faster (Wilkinson and Allen (2005)).

75 *2.3.2. Computer Architecture*

76 Parallel programs are commonly run on computer clusters. Computer clusters are a collection of
 77 nodes interconnected by a high speed communication network for message passing from one node to
 78 another. Analogously to a conventional PC each node as one or more CPUs and RAM. Commonly
 79 nodes are manufactured with two CPUs, each CPU is a multi-core meaning it has multiple compute
 80 cores that each can carry out calculations separately from one another. CPUs also have built in
 81 memory called cache that is much faster than RAM which is why for optimal performance cache
 82 utilization should be favoured over RAM when possible. On a node memory is divided by CPU
 83 sockets, so each CPU has direct access to memory local to its own socket, but accessing memory on
 84 another socket is much slower Jin et al. (2011). For this reason data that is needed for computation
 85 should be stored locally to the CPU that needs it.

86 Computer architectures are often classified by memory locality features. There are two distinct
 87 classes, distributed memory systems and shared memory systems. A cluster is a combination of the
 88 two classes. Each node operates its memory independently of the other nodes and explicit message
 89 passing is needed to share memory between nodes. While the cores on a node can operate in shared
 90 memory mode since memory updates can be made without explicit message passing statements from
 91 the user. All of these aspects of the computer architecture should be considered when designing a
 92 parallel program for the best performance (Adhianto and Chapman (2007)) maybe reword better
 93 to make more like CACE paper.

94 *2.3.3. Parallel Application Program Interfaces*

95 Message Passing Interface (MPI) is a common parallel computing application interface standard.
 96 MPI is used for distributed memory parallel computing, this is because MPI will operate every

97 MPI process as a discrete unit that does not share memory with the other processes unless explicit
98 message passing is used. Even on shared a single node where the hardware is supports shared
99 memory computing, MPI will still operate it in a distributed memory fashion Jin et al. (2011).
100 Operating all cores as distinct units also means they each need their own copy of all variables used
101 for computation which results in a large overall memory foot print compared to a same system if
102 it was operated in shared memory.

103 Open Multi-Processing (OMP) is another application program interface stand for parallel com-
104 puting. OMP is used for shared memory and can take advantage of shared memory systems which
105 can result in much faster computation. It does not work well on distributed systems though. This
106 prevents it from being used to efficiently carry out computations across multiple nodes of a cluster
107 simultaneously Jin et al. (2011).

108 Since MPI is best for distributed computing and OMP is better for shared computing many
109 individuals have studied the performance of MPI vs MPI+OMP methods and many studies have
110 used MPI+OMP for scientific computation for improved performance. Often times a trade off is
111 made between optimizing a program for performance and trying to make it flexible enough to run
112 on many different computer architectures [might need reference for this](#). A summary of some works
113 addressing MPI+OMP methods for scientific computing and architecture features and concerns can
114 be found in Bettencourt et al. (2017). In the conclusion to the work by Bettencourt et al. (2017) it
115 was found that hybrid methods for PBMs allow the code flexibility for different architectures while
116 still maintaining good performance. [should I mention load balancing techniques of gunawan paper?](#)?
117 In the work of Bettencourt et al. (2017) only the external(spatial) coordinates of the PBM were
118 parallelized. In this current work external and internal(compositions) calculations are parallelized.
119 [comment about how int and ext pll methods means better model for xyz reasons dotdotdot helps](#)
120 [to explicitly say reason](#)

121 3. Methods

122 3.1. DEM

123 3.1.1. LIGGGHTS

124 LIGGGHTSv3.60 (?) developed by DCS computing was used for all the simulation performed
125 in this study. Edits were made to the compute_contact_atom source file to obtain particle – particle
126 collisions. The aforementioned version of LIGGGHTS was compiled using the mvapich (mvapich2
127 v2.1) and intel (intel v15.0.2) compilers with the -o3 optimisation option as well as an option to
128 use OpenMP threads was implemented. This hybrid parallel technique helped achieve significant
129 speed improvements over MPI only compilations. The speed improvements are illustrated in Table
130 (refer to the speed table). The studies were performed on STAMPEDE supercomputer located at
131 University of Texas, Austin. The hardware configuration of each node consists of 2 8-core Intel
132 Xeon E5-2680 processors based on the Sandy Bridge architecture, 32 gb of memory with QPI
133 interconnects at 8.0 GT/s PCI-e lanes.

134 3.1.2. Geometry

135 [check other file Charles uploaded to see if that one was more "journal ready"](#)

136 In this study, the Lödige CoriMix CM5 continuous high shear granulator has been studied. Its
137 geometry was developed using the SolidWorksTM (Dassault Systèmes). This granulator consisted
138 of a high speed rotating element enclosed within a horizontal cylindrical casing. The casing (shown
139 in Figure 1) consists of a cylinder with diameter of 120 mm at the inlet and 130 mm at the outlet
140 and having a total length of 440 mm. A vertical inlet port is provided at one end of the casing and
141 an angled outlet port is provided at the larger end of the case.

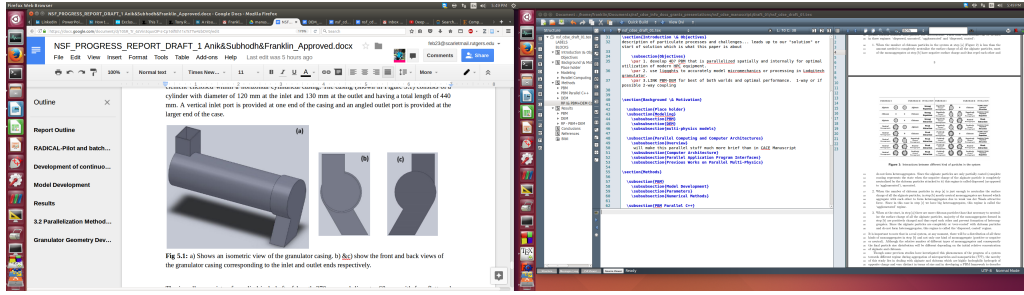


Figure 1: a) Shows an isometric view of the granulator casing. b) and c) show the front and back views of the granulator casing corresponding to the inlet and outlet ends respectively.

The impeller consists of a cylindrical shaft of length 370 mm and diameter 68 mm with four flattened sides 15 mm wide running along the axis. The blades are placed on these flattened sides as shown in figure 2. There are three different blade elements on the shaft (figure 2). At the granulator inlet, there are 4 paddle shaped feed elements following which there are 20 tear drop shaped shearing elements and finally 4 trapezoidal blades near the exit. All these elements are placed in a spiral configuration. The final configuration of the granulator is shown in figure 3.

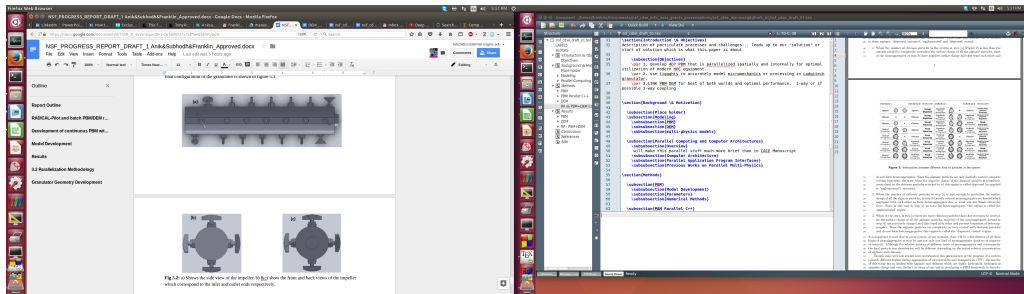


Figure 2: a) Shows the side view of the impeller. b) and c) show the front and back views of the impeller which correspond to the inlet and outlet ends respectively.

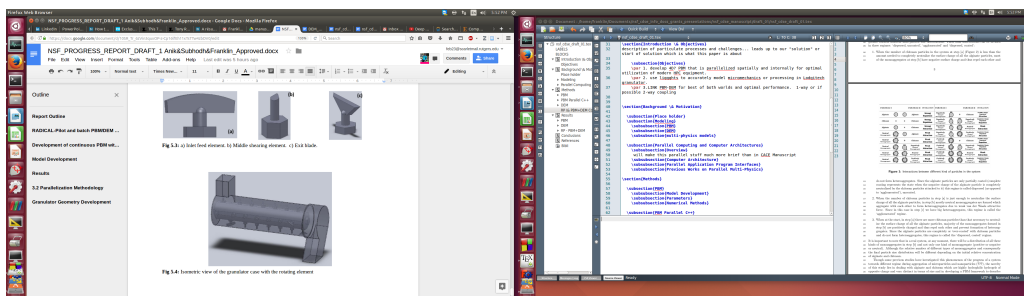


Figure 3: a) Inlet feed element. b) Middle shearing element. c) Exit blade. blah blah Isometric view of the granulator case with the rotating element

3.1.3. Meshing

After the geometry was built in solidworks the shell and impeller were exported as **non-binary** STL files. The coarsest output options(**include settings even if they were automatic may change from one version to another of SW**) were used to keep the STL files small and simple for faster computations times (**needs a citation? or is common knowledge?**). They were also exported not

153 keeping there original coordinates (1.too much info 2. what was option in SW for that so I can
154 use that wording) This resulted in the impeller having x-number-faces and y-number-points with
155 approximately a file size of number KBs. The shell had x-number-faces and y-number-points and
156 approx number KBs.

157 Meshlab was used to align the STL files for importing into LIGGGHTS. No mesh treatments
158 were used on the STLs.

159 The meshes were then imported into LIGGGHTS using the write command (more specific com-
160 mand that we actually used?). This resulted in 50 elements of the impeller file having "highly
161 skewed elements angles $| 0.5$ deg?" that according to LIGGGHTS would degrade parallel perfor-
162 mance. The shell did not have any skewed elements (FUTURE SOLUTION? - perhaps we can use
163 the output from liggghts exclusion list to find exact elements of issue. then we can use meshlab to
164 exclude those peices or remesh thos individual pieces into better shapes with less skewed elements.
165 might be better for a letter paper though

166 3.1.4. DEM input file settings

167 For the DEM simulations, a input script has to be prepared for LIGGGHTS. The input file
168 consists of various physical parameters of the particles being simulated, command lines for the
169 desired outputs from LIGGGHTS and various dump command which is used for post - processing
170 of the data.

171 Talk about mono and advantages and then psd. All the physical data is represented in the
172 Table 1

173 Need to add contact models, movement commands, all the start options,

174 3.1.5. DEM data post processing

175 The post processing of the data obtained from the DEM simulations was done using MATLAB®.
176 The first test run on the output data was to determine if the simulation had reached steady-state.
177 The mass inside the granulator was found out by averaging it over 5 time steps and then compared
178 to mass inside the granulator after every 10000 time steps (about 5×10^{-4} seconds) with a tolerance
179 of about 10

180 A precautionary script was also run so as to determine that no particles were lost due to overlap
181 of the geometry with the particles as well as from particle particle overlap.

182 3.2. PBM

183 3.2.1. Model Development

The main PBM equation developed for this work can be expressed as shown below:

$$\frac{d}{dt} F(s_1, s_2, x) = \mathfrak{R}_{agg}(s_1, s_2, x) + R_{break}(s_1, s_2, x) + \dot{F}_{in}(s_1, s_2, x) - \dot{F}_{out}(s_1, s_2, x) \quad (4)$$

184 citation?

185 where, $F(s_1, s_2, x)$ is the number of particles with an API volume of s_1 and an excipient volume
186 of s_2 in the spatial compartment x . The rate of change of number of particles with time in
187 different size classes depend on the rate of aggregation $\mathfrak{R}_{agg}(s_1, s_2, x)$ and the rate of breakage
188 $R_{break}(s_1, s_2, x)$. Also, the rate of particles coming into, $F_{in}(s_1, s_2, x)$ and going out, $F_{out}(s_1, s_2, x)$
189 of the spatial compartment due to particle transfer affect the number of particles in different size
190 classes. The rate of change of liquid volume is calculated using the equation:

[H]

Table 1: Physical Properties of the particle for the LIGGGHTS input script (Currently a placeholder)

Parameter	Symbol	Value	Units
Boltzmann constant	k	$1.3806488 \times 10^{-23}$	$m^2 \text{ kg s}^{-2} K^{-1}$
Charge of electron	e	$1.60217657 \times 10^{-19}$	Coulombs
Avogadro Number	N_A	6.0221413×10^{23}	—
Hamaker constant	A_H	3×10^{-21}	J
Hydration force constant	F_0	10^{-2}	$N m^{-1}$
Temperature of the medium	T	298	K
Viscosity of the medium	μ	0.8999×10^{-3}	Pa.s
Permittivity of the medium	$\epsilon_0 \epsilon_r$	6.93×10^{-10}	$C^2 N^{-1} m^{-2}$
Valence of ions in medium	z	1	—
Bulk concentration of ions in medium	C^b	1×10^{-2}	kg m^{-3}
Debye length	$\frac{1}{\kappa}$	1.3581×10^{-7}	m
Decay length	δ_0	6×10^{-10}	m
Density of alginate	$\rho_{Alginate}$	1050	kg m^{-3}
Density of chitosan	$\rho_{Chitosan}$	1000	kg m^{-3}
Surface potential of alginate	$\Psi_{Alginate}$	-46×10^{-3}	Volts
Surface potential of chitosan	$\Psi_{Chitosan}$	56×10^{-3}	Volts
Volume of the system	V	10×10^{-6}	m^3
Volume of the smallest alginate bin	a_1	1.5×10^{-17}	m^3
Volume of the smallest chitosan bin	c_1	0.3×10^{-17}	m^3
Aggregation kernel constant	K_0	5×10^9	—
Simulated Process Time	t	10	s
Simulation Time-Step	dt	0.01	s

$$\begin{aligned} \frac{d}{dt} F(s_1, s_2, x) l(s_1, s_2, x) = & \mathfrak{R}_{liq,agg}(s_1, s_2, x) + \mathfrak{R}_{liq,break}(s_1, s_2, x) + \dot{F}_{in}(s_1, s_2, x) l_{in}(s_1, s_2, x) \\ & - \dot{F}_{out}(s_1, s_2, x) l_{out}(s_1, s_2, x) + F(s_1, s_2, x) \dot{l}_{add}(s_1, s_2, x) \end{aligned} \quad (5)$$

where, $l(s_1, s_2, x)$ is the amount of liquid volume in each particle with API volume of s_1 and excipient volume of s_2 in the spatial compartment x . $\mathfrak{R}_{liq,agg}(s_1, s_2, x)$ and $\mathfrak{R}_{liq,break}(s_1, s_2, x)$ are respectively the rates of liquid transferred between size classed due to aggregation and breakage. $l_{in}(s_1, s_2, x)$ and $l_{out}(s_1, s_2, x)$ are respectively the liquid volumes of the particles coming in and going out of the spatial compartment. $l_{add}(s_1, s_2, x)$ is the volume of liquid acquired by each particle in the compartment at every time step due to external liquid addition.

Similarly, the rate of change of gas volume is calculated using the following equation:

$$\begin{aligned} \frac{d}{dt} F(s_1, s_2, x) g(s_1, s_2, x) = & \mathfrak{R}_{gas,agg}(s_1, s_2, x) + \mathfrak{R}_{gas,break}(s_1, s_2, x) + \dot{F}_{in}(s_1, s_2, x) g_{in}(s_1, s_2, x) \\ & - \dot{F}_{out}(s_1, s_2, x) g_{out}(s_1, s_2, x) + F(s_1, s_2, x) \dot{g}_{cons}(s_1, s_2, x) \end{aligned} \quad (6)$$

citation?

where, $g(s_1, s_2, x)$ is the gas volume of each particle with API volume of s_1 and excipient volume of s_2 in the spatial compartment x . $\mathfrak{R}_{gas,agg}(s_1, s_2, x)$ and $\mathfrak{R}_{gas,break}(s_1, s_2, x)$ are respectively

200 the rates of gas transferred between size classed due to aggregation and breakage. $g_{in}(s_1, s_2, x)$
 201 and $g_{out}(s_1, s_2, x)$ are respectively the gas volume of the particles entering and leaving the spatial
 202 compartment. $g_{cons}(s_1, s_2, x)$ is the volume of gas coming out of each particle in the compartment
 203 at every time-step due to consolidation of the particles.

The rate of aggregation, $\mathfrak{R}_{agg}(s_1, s_2, x)$ in Equation 4 is calculated as

$$\begin{aligned}\mathfrak{R}_{agg}(s_1, s_2, x) = & \frac{1}{2} \int_0^{s_1} \int_0^{s_2} \beta(s'_1, s'_2, s_1 - s'_1, s_2 - s'_2, x) F(s'_1, s'_2, x) F(s_1 - s'_1, s_2 - s'_2, x) ds'_1 ds'_2 \\ & - F(s_1, s_2, x) \int_0^{s_{max1}-s_1} \int_0^{s_{max2}-s_2} \beta(s_1, s_2, s'_1, s'_2, x) F(s'_1, s'_2, x) ds'_1 ds'_2\end{aligned}\quad (7)$$

204 **citation?**

where, the aggregation kernel, $\beta(s_1, s_2, s'_1, s'_2, x)$ is expressed as

$$\begin{aligned}\beta(s_1, s_2, s'_1, s'_2, x) = & \beta_o * (V(s_1, s_2, x) + V(s'_1, s'_2, x))^\gamma * (c(s_1, s_2, x) \\ & + c(s'_1, s'_2, x))^\alpha \left(1 - \frac{(c(s_1, s_2, x) + c(s'_1, s'_2, x))^\delta}{2}\right)^\alpha\end{aligned}\quad (8)$$

205 **citation?**

206 where, β_o , α , δ and γ are aggregation rate constants, $V(s_1, s_2, x)$ and $V(s'_1, s'_2, x)$ are the
 207 volumes of the aggregating particles. $c(s_1, s_2, x)$ and $c(s'_1, s'_2, x)$ are the external liquid fraction of
 208 the aggregating particles.

209 Similarly, the breakage rate is expressed as-

$$\mathfrak{R}_{break}(s_1, s_2, x) = \int_0^{s_{max1}} \int_0^{s_{max2}} K_{break}(s'_1, s'_2, x) F(s'_1, s'_2, x) ds'_1 ds'_2 - K_{break}(s_1, s_2, x) F(s_1, s_2, x)\quad (9)$$

210 **citation?**

211 where, the breakage kernel $K_{break}(s_1, s_2, x)$ is formulated as

$$K_{break}(s_1, s_2, x) = \left(\frac{4}{15\pi}\right)^{\left(\frac{1}{2}\right)} G_{shear} \exp\left(-\frac{B}{R(s_1, s_2, x)}\right)\quad (10)$$

212 **citation?**

213 where, G_{shear} is the shear rate exerted by the impeller on the granules. $R(s_1, s_2, x)$ is the
 214 radius of the granule that breaks and B is the breakage kernel constant. G_{shear} is calculated as
 215 $\frac{\nu_{impeller}*D_{impeller}*PI}{60}$ where $\nu_{impeller}$ and $D_{impeller}$ are respectively the rotational speed and diameter
 216 of the impeller.

217 The rate of increase of liquid volume of one particle, $\dot{l}_{add}(s_1, s_2, x)$ is expressed as $\frac{(s_1+s_2)(\dot{m}_{spray}(1-c_{binder})-\dot{m}_{evap})}{m_{solid}(x)}$
 218 where, $(s_1 + s_2)$ is the total solid volume of the particle; \dot{m}_{spray} is the rate of external liquid ad-
 219 dition, c_{binder} is the concentration of binder in the external liquid (which is assumed to be zero
 220 in this case as pure liquid is added); \dot{m}_{evap} is the rate of evaporation of liquid from the system
 221 (which is also assumed to be zero in this case) and m_{solid} is the total amount of solid present in
 222 the compartment.

223 The rate of decrease in gas volume per particle due to consolidation is calculated using the
 224 following expression:

$$\dot{g}_{cons}(s_1, s_2, x) = c * (\nu_{impeller})^\omega * V(s_1, s_2, x) \frac{(1 - \epsilon_{min})}{s} [g(s_1, s_2, x) + l(s_1, s_2, x) - (s_1 + s_2) \frac{\epsilon_{min}}{1 - \epsilon_{min}}] \quad (11)$$

where, c and ω are the consolidation constants; $\nu_{impeller}$ is the impeller rotational speed; $V(s_1, s_2, x)$ is the volume of particle, ϵ_{min} is the minimum porosity; $g(s_1, s_2, x)$ and $l(s_1, s_2, x)$ are respectively the gas and liquid volume of the particle.

Particle transfer rate, $F_{out}(s_1, s_2, x)$ in Equation 4 is calculated as $F(s_1, s_2, x) * \frac{\nu_{compartment(x)} * dt}{d_{compartment}}$ where, $\nu_{compartment(x)}$ and $d_{compartment}$ are respectively the average velocity of particles in compartment x and the distance between the mid-points of two adjacent compartment, which is the distance particles have to travel to move to the next spatial compartment. dt is the time-step. The values of various parameters used in the model are provided in Table 2.

Table 2: Parameters for PBM from Anik's hetero. agg. paper. currently place holder

Parameter	Symbol	Value	Units
Boltzmann constant	k	$1.3806488 \times 10^{-23}$	$m^2 \text{ kg s}^{-2} K^{-1}$
Charge of electron	e	$1.60217657 \times 10^{-19}$	Coulombs
Avogadro Number	N_A	6.0221413×10^{23}	—
Hamaker constant	A_H	3×10^{-21}	J
Hydration force constant	F_0	10^{-2}	$N m^{-1}$
Temperature of the medium	T	298	K
Viscosity of the medium	μ	0.8999×10^{-3}	Pa.s
Permittivity of the medium	$\epsilon_0 \epsilon_r$	6.93×10^{-10}	$C^2 N^{-1} m^{-2}$
Valence of ions in medium	z	1	—
Bulk concentration of ions in medium	C^b	1×10^{-2}	$kg m^{-3}$
Debye length	$\frac{1}{\kappa}$	1.3581×10^{-7}	m
Decay length	δ_0	6×10^{-10}	m
Density of alginate	$\rho_{Alginate}$	1050	$kg m^{-3}$
Density of chitosan	$\rho_{Chitosan}$	1000	$kg m^{-3}$
Surface potential of alginate	$\Psi_{Alginate}$	-46×10^{-3}	Volts
Surface potential of chitosan	$\Psi_{Chitosan}$	56×10^{-3}	Volts
Volume of the system	V	10×10^{-6}	m^3
Volume of the smallest alginate bin	a_1	1.5×10^{-17}	m^3
Volume of the smallest chitosan bin	c_1	0.3×10^{-17}	m^3
Aggregation kernel constant	K_0	5×10^9	—
Simulated Process Time	t	10	s
Simulation Time-Step	dt	0.01	s

3.2.2. Parameters

3.3. PBM Parallel C++

3.3.1. Discretization & Parallelizing PBM

The PBM was discretized by converting each of its coordinates in to discrete bins. For the spatial coordinates a linear bin spacing was used. For the internal coordinates, solid,liquid, and gas

238 a nonlinear binning was used. get more details from Anik on this will probably need more detail
239 on binning for reproducability

240 Once the PBM had been discretized (compartmentalized/binned) a finite differences method was
241 used which created a system of ordinary differential equations (ODEs). The numerical integration
242 technique used to evaluate the system of ODEs was first order Euler integration check with Anik
243 that is what we used as it is commonly used to solve these types of systems and author found it
244 improved speeds while having minimal impact on accuracy. To obtain the most optimal parallel
245 performance, when solving the PBM, work loads were distributed in a manner which took into
246 account the shared memory and distributed memory aspects of the clusters the PBM was being
247 run on. To parallelize the model in a way which could take advantage of shared memory but still
248 effectively run across a distributed system both OMP and MPI were implemented.

249 One MPI process was used per CPU socket and one OMP process was used per CPU core, as
250 authors (Bettencourt et al. (2017)) found it resulted in the best performance. MPI was used for
251 message passing from one node to another while OMP was used for calculations on each node that
252 could be efficiently solved using a shared memory system i.e. calculations were inter-dependent but
253 could be computed simultaneously.

254 Pseudo code is presented below illustrating how the calculations are distributed and carried out
255 during the simulation. For each time step the MPI processes are made responsible for a specific
256 chunk of the spatial compartments. Then each OMP thread, inside of each MPI process, is allocated
257 to one of the cores of the the multi-core CPU the MPI process is bound too. The OMP processes
258 divide up and compute \mathfrak{R}_{agg} and \mathfrak{R}_{brk} . (include more detail about how they do it? last paper
259 reviewer complained that could not understand figure by JUST reading what I wrote about it in
260 meat of paper)

261 After \mathfrak{R}_{agg} and \mathfrak{R}_{brk} are calculated the MPI processes calculate the new PSD value for their
262 chunk at that specific time step, $F_{t,c}$. The slave processes send their $F_{t,c}$ to the master processes
263 which collects them into the complete $F_{t,all}$. The master process then broadcasts the $F_{t,all}$ value to
264 all slave processes.

265 A crucial feature of the PBM is that the current PSD ($F_{t,all}$) value is used to compute a new
266 time step size for the next iteration. This means all of the MPI processes need to have the same
267 dynamic time step size at each iteration for the calculations to be properly carried out in parallel.
268 Since the completely updated $F_{t,all}$ value is shared before calculating a new time step each process
269 will have the same $F_{t,all}$ value. As a result each process calculates the same size for the new time
270 step. Did not include the liquid and gas PBMs in this but hoping they will be some what assumed?
271 Also the Ragg omp distributed work is an a what about private OMP vars specified that has impact
272 on how model is solved etc. Should look into this. might change based on locking/blocking tests
273 that need to be implemented still.

Algorithm 1 Pseudo code

```

while  $t < t_{final}$  do
    // the spatial domain is divided into equal chunks (with in 1 bin size)
    // each MPI process is assigned on chunk of spatial domain shown as  $c_{low}$  to  $c_{up}$ 
    // sum all  $c_{low_i}$  to  $c_{up_i}$  is = to [0,numCompartments]
    for each MPI processes do  $c = c_{low_i}$  to  $c_{up_i}$ 
        // each MPI process is further divided with OMP to take advantage of multi-core CPU
        // each OMP process is allocated to a single compute core
        //  $\Re$  integrals (i1)  $\int_0^{s_2}$ , (i2)  $\int_0^{s_{max2}-s_2}$ , and (i3)  $\int_0^{s_{max2}-s_2}$  are divided into smaller integrals
        //  $\int_{i_1 low_n}^{i_1 up_n}$ ,  $\int_{i_2 low_n}^{i_2 up_n}$ , and  $\int_{i_3 low_n}^{i_3 up_n}$  which are solved by the "n" OMP processes
        // allocated to that MPI process (CPU)
        for each OMP process do

            
$$\Re_{agg}(s_1, s_2, c) = \frac{1}{2} \int_0^{s_1} \int_{i_1 low_n}^{i_1 up_n} \beta(s'_1, s'_2, s_1 - s'_1, s_2 - s'_2, c) F(s'_1, s'_2, c) F(s_1 - s'_1, s_2 - s'_2, c) ds'_1 ds'_2$$

            
$$- F(s_1, s_2, c) \int_0^{s_{max1}-s_1} \int_{i_2 low_n}^{i_2 up_n} \beta(s_1, s_2, s'_1, s'_2, c) F(s'_1, s'_2, c) ds'_1 ds'_2$$


            
$$\Re_{break}(s_1, s_2, c) = \int_0^{s_{max1}} \int_{i_3 low_n}^{i_3 up_n} K_{break}(s'_1, s'_2, c) F(s'_1, s'_2, c) ds'_1 ds'_2 - K_{break}(s_1, s_2, c) F(s_1, s_2, c)$$


        end for

        
$$F_{t,c} = \frac{\Delta F(s_1, s_2, c)}{\Delta t} \Delta t + F(s_1, s_2, c)_{t-1}$$

        
$$= (\Re_{agg}(s_1, s_2, c) + \Re_{break}(s_1, s_2, c) + \dot{F}_{in}(s_1, s_2, c) - \dot{F}_{out}(s_1, s_2, c)) \Delta t + F(s_1, s_2, c)_{t-1}$$


    end for
    MPI Send  $F_{t,c}$  to Master MPI process
    MPI Recv  $F_{t,c}$  from MPI all slave processes
    Master consolidate all  $F_{t,c}$  chunks into a complete  $F_{t,all}$ 
    Master does inter-bin particle transfers (updates  $F_{t,all}$ )
    MPI Broadcast  $F_{t,all}$  to all slave processes
     $t_{new} = t + timestep$ 
end while

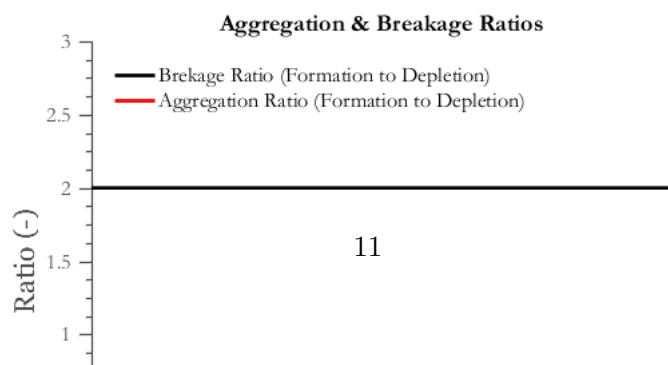
```

274 3.4. RP & PBM+DEM Communication

275 **4. Results**

276 **4.1. PBM**

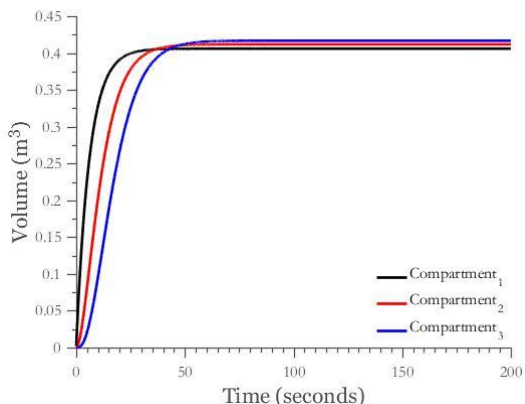
277 **4.1.1. PBM Validation**



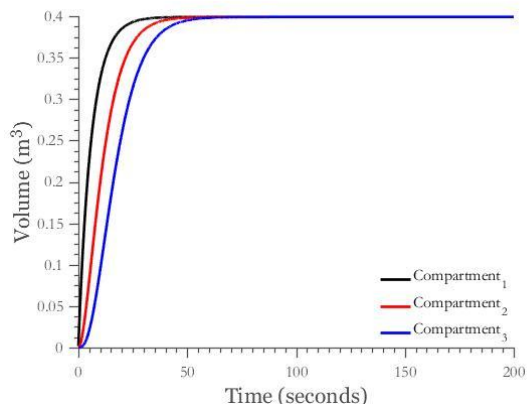
278 The ratio between the number of particles formed due to aggregation and the number of particles
279 depleted due to aggregation and the ratio of the number of particles formed due to breakage to the
280 number of particles depleted due to breakage are plotted. In aggregation two particles agglomerate
281 to form one particle and in breakage one particle breaks to form two particles. So, these ratios
282 are expected to be 0.5 and 2 respectively. As can be seen from Figure 4, these ratios are accurate
283 confirming that mass is conserved accurately in the model.

284 The granulator was divided into 3 compartments spatially and the total volume, solid volume
285 and pore volume and the median diameter d_{50} in each compartment were plotted to study the
286 granulation behaviour and are shown in Figure 5.

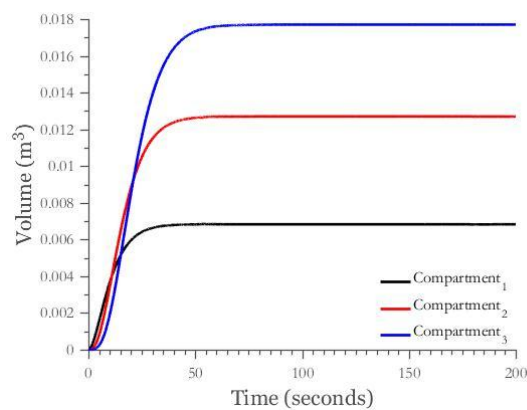
287 It can be seen from Figure 5a that the total volume starts to increase first in compartment 1
288 followed by compartment 2 and then compartment 3. This happens as gradually particles entering
289 compartment 1 moves to the other compartment due to particle transfer from compartment 1 to
290 compartment 2 and then compartment 3. In Figure 5b it is observed that the solid volume similar
291 to the total volume increases first in compartment 1 and last in compartment 3. The solid volume
292 becomes constant and equal in all the compartments at around 30-50 seconds and steady state is
293 reached when the rate of particle volume being transported through the compartments and leaving
294 the system is equal to the rate of particles entering the system. Although, as seen in Figure 5c
295 the pore volume which is the sum of the gas and the liquid volume is highest in compartment 3
296 and lowest in compartment 1. This happens due to the external liquid addition to the system. As
297 the particles move from compartment 1 to compartment 3, they gradually acquire a higher amount
298 liquid, thereby increasing the pore volume. In Figure 5d, the D_{50} is seen to be increasing from
299 compartment 1 to 3. This happens because of the size enlargement of large particles coming in
300 from the previous compartment because of the external liquid added to each compartment and a
301 longer residence time in the granulator.



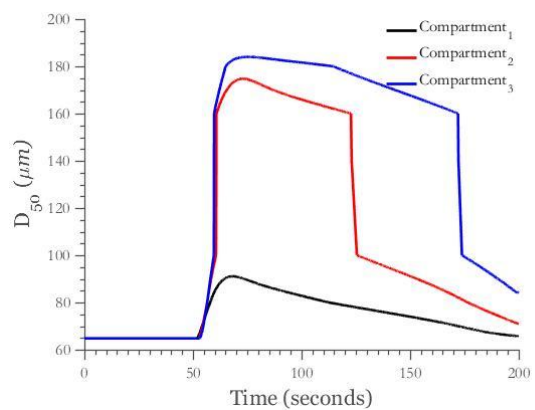
(a) Total volume in all compartments



(b) Total solid volume in all compartments



(c) Total pore volume in all compartments



(d) D_{50} in all compartments

Figure 5: Volume and D_{50} in all compartments over time. Volumes become constant as steady state is reached. Median diameter increases and then decreases as bigger particles leave the system and smaller particles occupy that volume.

302 4.1.2. Parallel C++ PBM Validation

303 show PSD or D_{50} is the same as Matlab or serial PBM

304 1. fig D_{50} Matlab vs Parallel

305 4.1.3. Parallel PBM Performance

306 show that RP has minimal impact on performance

307 show that performance is mostly unaffected by RP

308 1. fig scaling

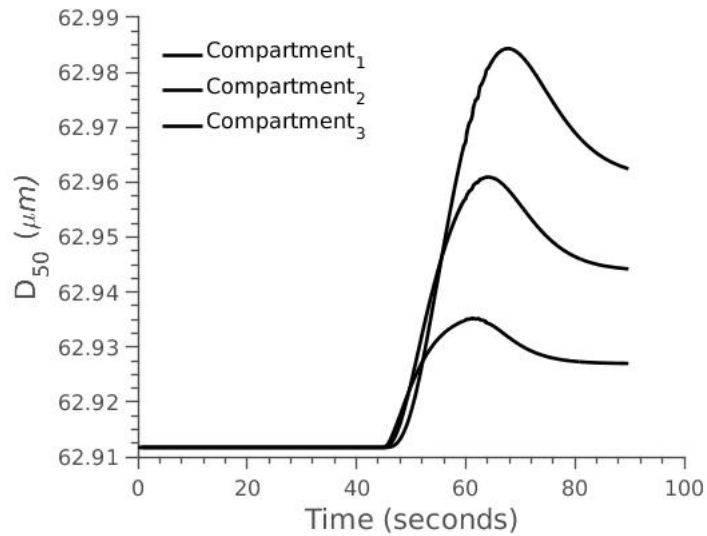


Figure 6: D_{50} of Matlab PBM vs Parallel PBM

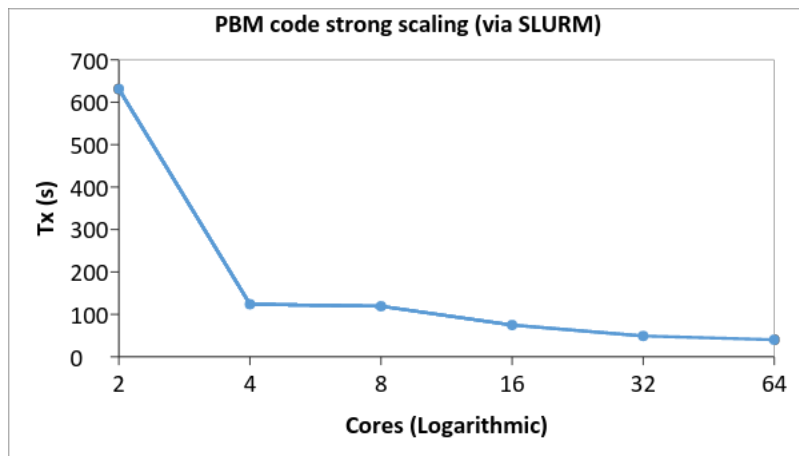


Figure 7: PBM strong scale slurm

309 2. fig scaling w/ RP

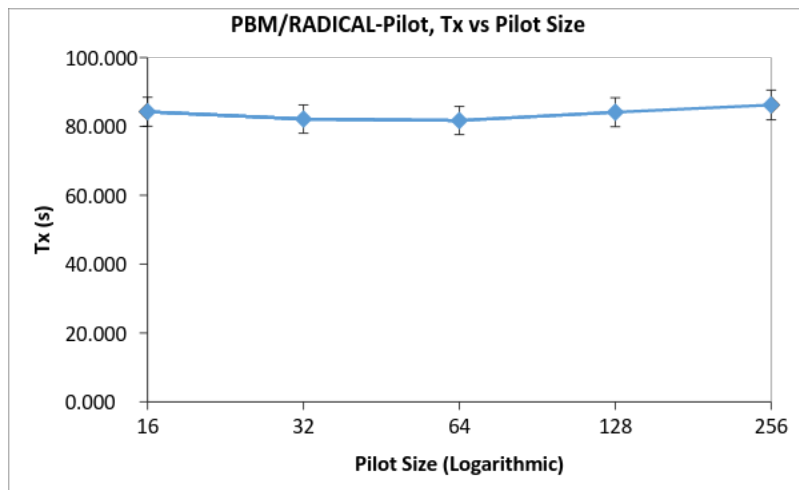


Figure 8: PBM strong scale RP

310 4.1.4. Parallel PBM Parameter space and Parameter Estimation

- 311 I. show how effective parallel pbm is for parameter estimation
- 312 II. Find/ explore ranges of DEM data that PBM can use to find Critical parameters and
- 313 sensitivities will be useful to us in linking and in picking best DEM parameters to vary and best
- 314 parameters for PBM+DEM code
 - 315 1. fig range of some parameters?
 - 316 2. fig range of other pbm parameter ?

317 4.2. DEM

318 4.2.1. DEM Validation and Parameter Space Studies

- 319 show that DEM is somewhat behaving like a real system
- 320 fig constant flow reached by end of DEM simulation

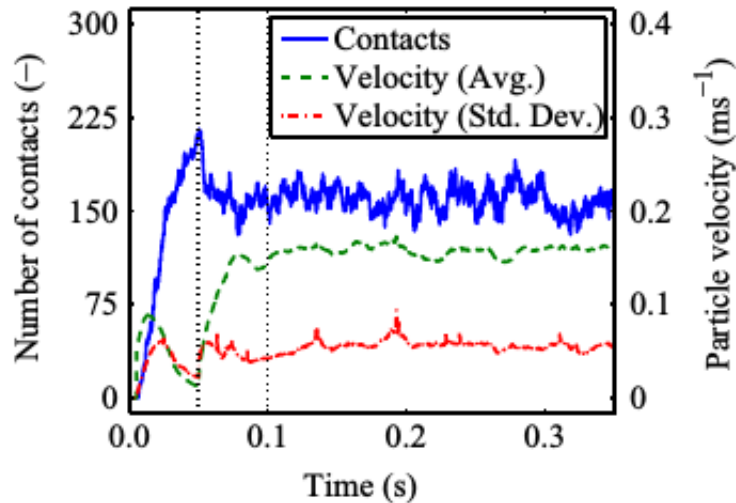


Fig. 3. Time trajectories from DEM simulation showing number of contacts between 1-mm particles with particles of the same size, and the average and standard deviation of the velocity of 1-mm particles. Particles are added at time=0 s with a median diameter of 1.5 mm and a standard deviation of 0.5 mm. Dotted lines indicate start of rotation of the screw and start of data collection, respectively.

Figure 9

321 fig RTD
 322 show affects of certain parameters on DEM and which ones are most critical to outcomes - will
 323 help decide on PBM+DEM parameters to study in later section
 324 fig vary impeller RPM see how RTD or hold up changes
 325 fig vary PSD (range and/or particle sizes) to see how C_{coll} etc will be affected - important for
 326 PBM Kernel

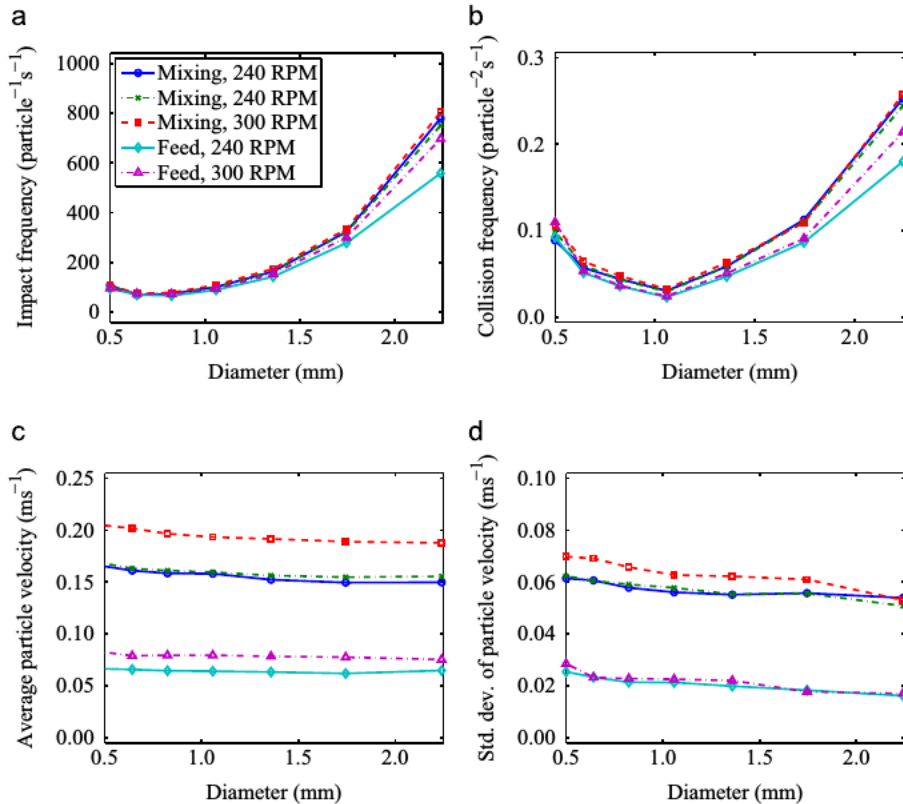


Fig. 6. DEM results showing the effects of screw element type and rotational speed on (a) impact frequency, (b) collision frequency with 1-mm particles, (c) average particle velocity, and (d) standard deviation of particle velocity for each size class.

Figure 10: fig showing sensitivity of C_{coll} and etc to RPM

327 fig vary impeller RPM see C_{coll} changes

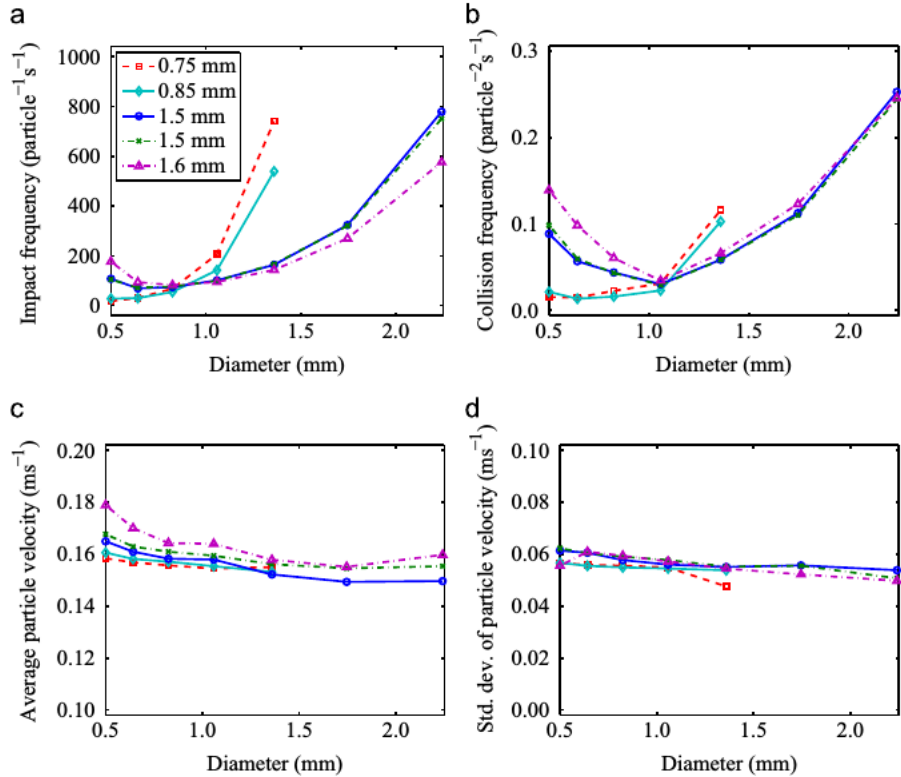


Fig. 4. DEM results showing the effects of size distribution on (a) impact frequency, (b) collision frequency with 1-mm particles, (c) average particle velocity, and (d) standard deviation of particle velocity for each size class. Median diameters are listed in the legend. The standard deviation of the diameter is fixed at 0.2 mm for the smallest two simulations and 0.5 mm for the larger simulations.

Figure 11: fig from dana 2015 mechanistic bi-directional

328 4.2.2. DEM Performance

329 show that performance is mostly unaffected by RP
 330 1. fig scaling

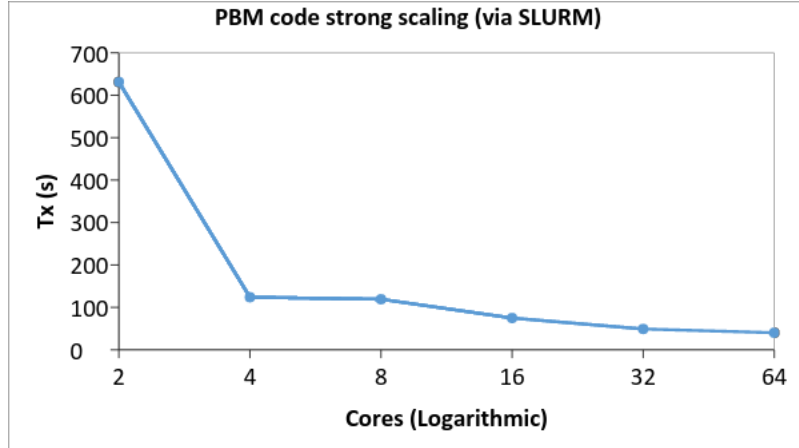


Figure 12: DEM scale just slurm

331 2. fig scaling w/ RP

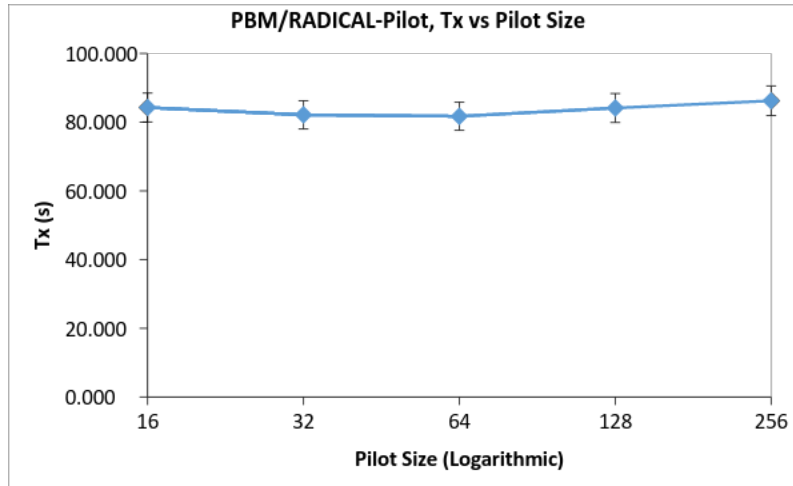


Figure 13: DEM scale with RP

332 4.3. PBM+DEM - RP

333 4.3.1. PBM+DEM Validation/Accuracy?

334 4.3.2. PBM+DEM Performance

335 strong scaling

fig PBM + DEM RP strong scaling

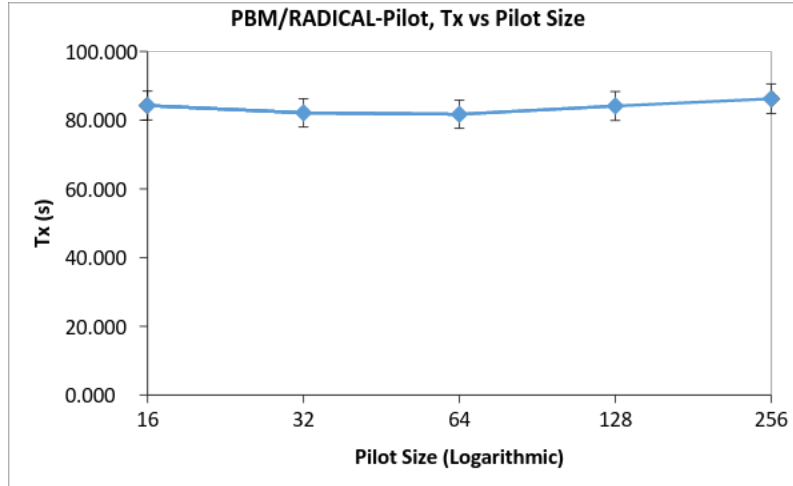


Figure 14: PBM+DEM scale with RP

336

337 4.3.3. PBM+DEM Parameter studies

338 show how PBM+DEM captures multi-physics as parameters changed. helps validate and support model development. show we have made a useful tool for future work.

340 fig

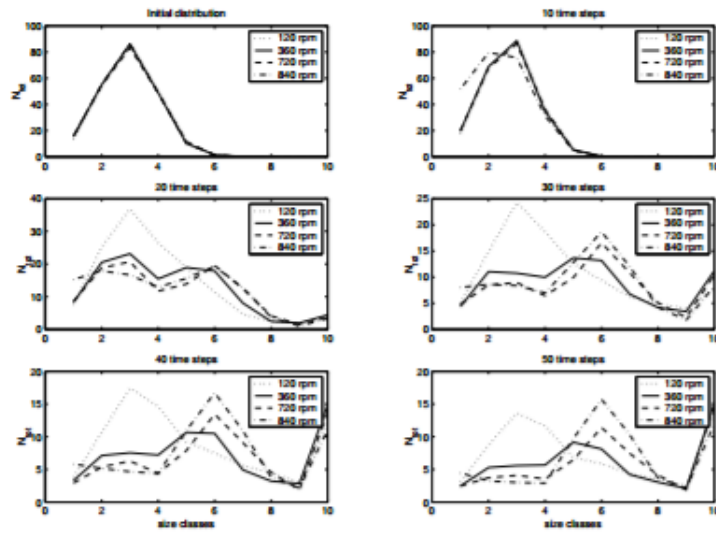


Figure 8: PSD evolution for simulations run at 120 rpm, 360 rpm, 720 and 840 rpm.

Figure 15: PBM+DEM scale with RP

341 PSD over time for different impeller RPM

342 **5. Conclusions**

343 **References**

- 344 Adhianto, L., Chapman, B., 2007. Performance modeling of communication and computation in
345 hybrid {MPI} and openmp applications. Simulation Modelling Practice and Theory 15 (4), 481
346 – 491, performance Modelling and Analysis of Communication Systems.
347 URL <http://www.sciencedirect.com/science/article/pii/S1569190X06001109>
- 348 Barraso, D., Ramachandran, R., 2015. Multi-scale modeling of granulation processes: Bi-
349 directional coupling of {PBM} with {DEM} via collision frequencies. Chemical Engineering Re-
350 search and Design 93, 304 – 317.
351 URL <http://www.sciencedirect.com/science/article/pii/S0263876214001920>
- 352 Barraso, D., Walia, S., Ramachandran, R., 2013. Multi-component population balance modeling of
353 continuous granulation processes: A parametric study and comparison with experimental trends.
354 Powder Technology 241, 85 – 97.
355 URL <http://www.sciencedirect.com/science/article/pii/S0032591013001666>
- 356 Bettencourt, F. E., Chaturbedi, A., Ramachandran, R., 2017. Parallelization methods for efficient
357 simulation of high dimensional population balance models of granulation. Computers & Chemical
358 Engineering, –.
359 URL <http://www.sciencedirect.com/science/article/pii/S0098135417301072>
- 360 Cundall, P. A., Strack, O. D. L., 1979. A discrete numerical model for granular assemblies. Gotech-
361 nique 29 (1), 47–65.
362 URL <http://dx.doi.org/10.1680/geot.1979.29.1.47>

- 363 Jin, H., Jespersen, D., Mehrotra, P., Biswas, R., Huang, L., Chapman, B., 2011. High performance
364 computing using {MPI} and openmp on multi-core parallel systems. Parallel Computing 37 (9),
365 562 – 575, emerging Programming Paradigms for Large-Scale Scientific Computing.
366 URL <http://www.sciencedirect.com/science/article/pii/S0167819111000159>
- 367 Ramachandran, R., Immanuel, C. D., Stepanek, F., Litster, J. D., III, F. J. D., 2009. A mecha-
368 nistic model for breakage in population balances of granulation: Theoretical kernel development
369 and experimental validation. Chemical Engineering Research and Design 87 (4), 598 – 614, 13th
370 European Conference on Mixing: New developments towards more efficient and sustainable op-
371 erations.
372 URL <http://www.sciencedirect.com/science/article/pii/S0263876208003225>
- 373 Ramkrishna, D., Singh, M. R., 2014. Population Balance Modeling: Current Status and Future
374 Prospects. Annual Review of Chemical and Biomolecular Engineering 5 (1), 123–146.
375 URL <http://dx.doi.org/10.1146/annurev-chembioeng-060713-040241>
- 376 Wilkinson, B., Allen, C., 2005. Parallel Programming: Techniques and Applications Using Net-
377 worked Workstations and Parallel Computers. An Alan R. Apt book. Pearson/Prentice Hall.
378 URL <https://books.google.com/books?id=F8C2QgAACAAJ>